Journal of Glaciology

Paper

Cite this article: Petersen EI, Levy JS, Holt JW, Stuurman CM (2020). New insights into ice accumulation at Galena Creek Rock Glacier from radar imaging of its internal structure. *Journal of Glaciology* **66**(255), 1–10. https://doi.org/10.1017/jog.2019.67

Received: 8 June 2019
Revised: 1 August 2019
Accepted: 7 August 2019
First published online: 4 October 2019

Keywords:
Accumulation; debris-covered glaciers; glacier geophysics; supraglacial debris

Author for correspondence:
Eric Ivan Petersen, E-mail: petersen@lpl.arizona.edu

cambridge.org/jog

New insights into ice accumulation at Galena Creek Rock Glacier from radar imaging of its internal structure

Eric Ivan Petersen[1,2], Joseph S. Levy[3], John W. Holt[1] and Cassie M. Stuurman[4]

[1]Lunar and Planetary Laboratory, University of Arizona, AZ, USA; [2]University of Texas Institute for Geophysics, University of Texas at Austin, Austin, TX, USA; [3]Colgate University, NY, USA and [4]European Space Agency, Noordwijk, The Netherlands

Abstract

The ice-cored Galena Creek Rock Glacier, Wyoming, USA, has been the subject of a number of studies that sought to determine the origin of its ice. We present new observations of the rock glacier's internal structure from ground-penetrating radar to constrain ice and debris distribution and accumulation. We imaged dipping reflectors in the center of the glacier that are weak and discontinuous, in contrast to strong reflectors toward the edge of the cirque beneath large debris-avalanche chutes. These reflectors form a network of concave-up, up-glacier dipping layers. We interpret these as englacial debris bands formed by large debris falls buried by subsequent ice and snow accumulation. They are discontinuous where ice outpaces debris accumulation, but with sufficient debris accumulation an interleaved pattern of ice and debris layers can form. We propose a model in which the ice in these interleaved layers is snowfall preserved by debris-facilitated accumulation. Large debris falls that occur in early spring bury sections of the snowpack, which are then preserved through summer and incorporated into the rock glacier body over time. This study highlights the importance of sequential accumulation of ice and debris for understanding the dynamics of rock glaciers and debris-covered glaciers.

Introduction

Galena Creek Rock Glacier is a site of great importance in the rock glacier scientific literature, being a touchstone in the historical debate around rock glacier origins (Potter and others, 1998). Rock glaciers are found in alpine and polar environments and are defined by a surface of talus debris that exhibits morphologic evidence for viscous flow. This can include an oversteepened toe (often at the angle of repose of the debris), flow-parallel lineations/boulder trains similar to medial moraines and transverse ridges (Capps, 1910; Wahrhaftig and Cox, 1959).

Hypotheses of rock glacier formation generally fall into two categories: those maintaining that many rock glaciers are cored with snowfall-derived glacial ice (Potter, 1972) and those maintaining that rock glaciers are exclusively periglacial features with interstitial ice sourced from refreezing of meteoric water and snow/ice melt (Barsch, 1987). In their seminal survey of 200 rock glaciers in the Alaska Range, Wahrhaftig and Cox (1959) presented the periglacial model, in which observed interstitial rock glacier ice is accumulated by the refreezing of snowmelt and rainwater percolated into talus debris in periglacial environments. In contrast, Outcalt and Benedict (1965) studied a number of rock glaciers in the Colorado rockies and drew a distinction between two types: (1) tongue-shaped cirque floor rock glaciers containing pure ice cores that they hypothesized are the debris-covered snouts of former glaciers and (2) apron-shaped valley wall rock glaciers containing interstitial ice that they hypothesized is avalanche snow buried by debris fall.

To date, there has been ample evidence for glacial ice-cored rock glaciers, while periglacial processes may still play a role in some localities (Clark and others, 1998). An example of the former is the study of Galena Creek Rock Glacier by Potter (1972), who used exposure observations and seismic profiling to show that the glacier in the upper two-thirds of the valley is cored by 88–90% purity sedimentary ice under a surface debris layer 1–1.5 m thick.

Because rock glaciers can preserve large quantities of ice they are of interest as significant components in alpine and polar hydrological systems (Rangecroft and others, 2015) and as unique records of climate history (Steig and others, 1998). Rock glaciers also receive attention from the planetary science community as analogs to martian landforms with similar morphology (Squyres, 1978; Mahaney and others, 2007; Holt and others, 2008; Petersen and others, 2018). For each of these applications it is important to understand the ice accumulation mechanisms for rock glaciers.

Potter (1972) used observations of snowfield depth and debris fall at Galena Creek Rock Glacier to hypothesize that ice is formed by accumulation of wind-blown snow in a narrow accumulation zone at the base of cirque headwalls. The ice is then preserved by debris fall coming to rest on the snow surface at the downslope margin of the accumulation zone, leaving little debris to be entrained in the glacier ice.

Anderson and others (2018) presented a model of rock glaciers as an end-member of debris-covered glaciation, with ice accumulated via avalanche cones where the equilibrium

line altitude is above the surrounding topography. Avalanche cones are formed by wind-loading of snow in the lee side of alpine ridges, and preserved preferentially on more shaded slopes where summer ablation is unable to remove all deposited snow. Debris is delivered to the system via rock fall that may come to a rest past the accumulation zone (as in Potter, 1972) or be entrained in the avalanche cones, to be melted out in the ablation zone.

The models presented by Potter (1972) and Anderson and others (2018) stand in contrast to a debris-covered glacier model developed by Mackay and others (2014). In the model of Mackay and others (2014), the bulk of the ice is deposited during periods of net positive ice accumulation while the glacier-wide surface debris lag is formed during periods of net ablation. This model leads to the possibility of buried debris layers that may record ice accumulation cycles and thus climate history.

On the periglacial end of the spectrum, a number of studies have hypothesized that seasonal snowpack, avalanche cones and ice-rich soils are periodically covered by talus debris fall and thus entrained within rock glaciers as ice-rich lenses (Berthling and others, 2000; Isaksen and others, 2000; Degenhardt and Giardino, 2003).

Geophysical methods provide a powerful tool for constraining the bulk composition and internal structure of rock glaciers, which can be used to test for formation mechanisms. Hauck and others (2011) developed a model for constraining the four-way ice, debris, water and air content of rock glacier material from electrical resistivity and seismic p-wave velocity data. Ground-penetrating radar (GPR) is a particularly useful technique for imaging interfaces in the subsurface of rock glaciers and debris-covered glaciers, including englacial debris layers and the base of the ice (Degenhardt and Giardino, 2003; Florentine and others, 2014; Mackay and others, 2014). These methods have additionally been integrated with gravimetry (Hausmann and others, 2007) and transient electromagnetic (Maurer and Hauck, 2007) to provide a holistic view of the bulk composition of layers within the rock glacier, as well as its finer-scale internal structure.

Motivated by the goal of constraining ice and debris accumulation history at Galena Creek Rock Glacier, we present a GPR survey performed at the site designed to image the rock glacier's internal structure. Specifically, we tested Potter's accumulation hypothesis and searched for possible climate signals.

Study site

Galena Creek Rock Glacier is located in a north-facing valley in the Absaroka Mountains of northern Wyoming (Fig. 1). It is 240–300 m wide and stretches 1.6 km from the cirque at an elevation of 3100 m to its toe at an elevation of 2700 m. The rock glacier is composed of a core of pure glacial ice in the upper two-thirds of the valley, based on ice exposure observations (Potter, 1972; Potter and others, 1998) and recovered ice cores (Clark and others, 1996; Konrad and others, 1999). The rock glacier in the lower third of the valley is inferred from seismic refraction velocities to contain only an ice–rock mixture (Potter and others, 1998). The surface debris layer, composed of boulders eroded from headwall bedrock, has been measured at 1–1.5 m thick for the upper section and 2–3 m thick for the lower section (Potter, 1972). Ice has successfully been cored down to 25 m depth in the upper section (Clark and others, 1996; Konrad and others, 1999).

Ackert (1998) mapped the gross geomorphology of Galena Creek Rock Glacier and identified lateral ice-cored moraines based on their reduced flow speeds, increased lichen cover and flow-longitudinal ridges. He associated these mapped lateral moraines with individual rock glacier lobes and hypothesized that they correspond to the extent of previous glacier lobes during periods of higher positive mass balance. We have included this mapping in Figure 1 as a reference.

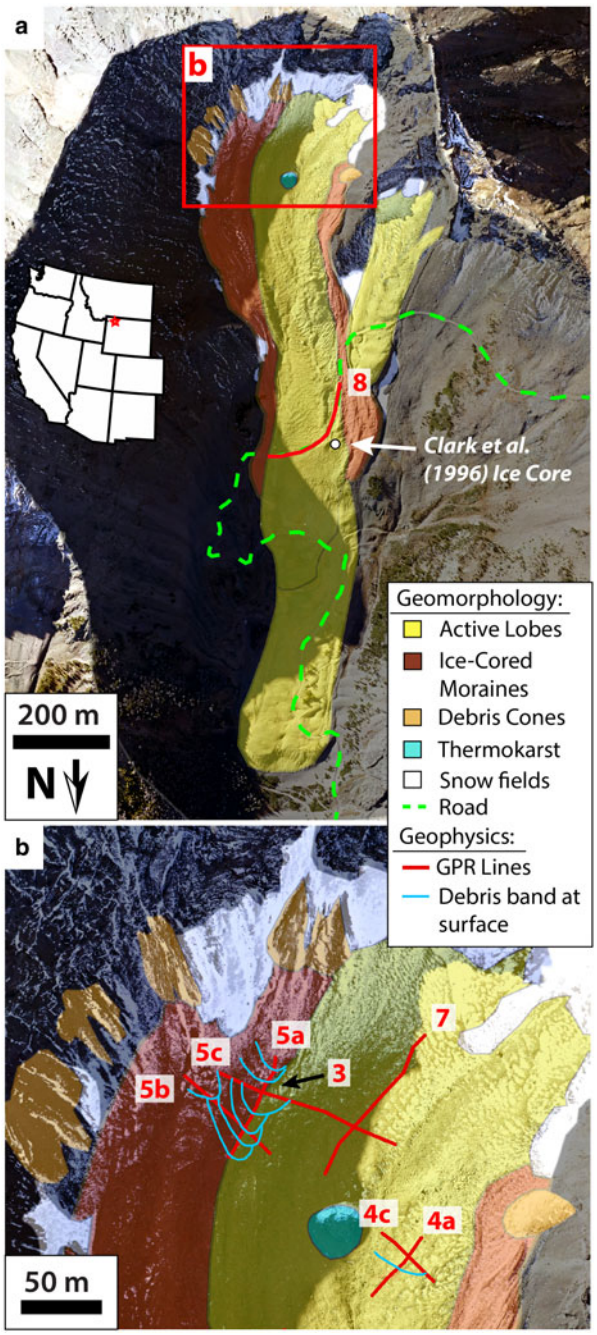

Fig. 1. (a) Orthorectified airborne image of Galena Creek Rock Glacier overlain by geomorphic mapping based on the work of Ackert (1998); the location of the ice core of Clark and others (1996), the forest service road and the radargram in Figure 8 are also mapped. The location of the site is shown in an inset map of the western United States. (b) Detail of the cirque showing the location of the thermokarst pond and the radargrams shown in Figures 4, 5 and 7. Radar observation 3 (a common midpoint survey) is centered on the intersection of the lines indicated by the black arrow. An interpretation of where strong dipping reflectors in GPR data intersect the surface is mapped in purple. North is to the bottom of the figure.

Potter and others (1998) measured surface velocities by surveying surface boulder displacement over a period of 28–32 years and found that typical velocities range between 16–45 cm a^{-1}, with a maximum of 80 cm a^{-1} observed on the steep slope below the cirque. Seismic refraction surveys by Potter and others (1998) inferred the basal contact between glacier ice and bedrock to be at depths of up to 20–25 m. Based on a comparison between this glacial thickness and Glen's flow law (Nye, 1957), Potter and others (1998) inferred that as much as half of the glacier

velocity may be attributable to basal sliding. In contrast, Konrad and others (1999) presented an expanded velocity dataset to produce distributed thickness estimates from Glen's flow law and found values consistent with depths found by ice coring sites, thus arguing that there is no need for basal sliding or debris deformation.

The debris cover of Galena Creek Rock Glacier is composed of boulders eroded from bedrock in the headwall. The bedrock geology in the locale of Galena Creek Rock Glacier is defined by the Wapiti Formation, which is composed of dark andesitic volcaniclastic rocks consisting entirely of vent facies (Smedes and Prostka, 1972). There are also numerous lighter-colored dikes and intrusions.

Methods

We made general observations of a thermokarst pond found in August 2015 in the upper cirque portion of Galena Creek Rock Glacier. The walls of this pond exposed the upper several meters of the internal structure of the rock glacier, which allowed us to ground-truth our geophysical survey. A tape measure was used to measure the gross morphology of the pond and its exposure, a Brunton compass was used to measure the apparent dip of surfaces, and photographs, notes and sketches were taken.

We conducted GPR surveys at 50 and 100 MHz using a Sensors and Software PulseEKKO Pro system. GPR is a powerful tool in the field of glaciology and has been used widely to survey rock glaciers (e.g. Degenhardt and Giardino, 2003; Hausmann and others, 2007; Maurer and Hauck, 2007; Florentine and others, 2014) We employed GPR as our chief method due to relatively higher ease and speed of data acquisition compared with other geophysical methods, as well as its particular strength in imaging englacial interfaces and fine-scale structure. Over two field seasons in August 2015 and August 2016 we collected 12 reflection surveys and one common midpoint survey. The common midpoint survey and eight reflection surveys were obtained in the cirque, while the three remaining reflection surveys were obtained in the middle section of the glacier (see Fig. 1). Diffraction hyperbolae were fit to each of the reflectors observed in the common midpoint survey to determine the radio wave velocity as a function of depth. Each of the reflection surveys were then migrated and corrected to depth using the determined radio wave velocity.

We produced a digital elevation model (DEM) at a resolution of 17 cm px^{-1} via airborne photogrammetry and used it to correct GPR data for topography. Images were collected using a Canon EOS 5D Mark III camera with an EF50mm lens from a vibration-stabilized nadir-looking mount in a modified Kestral Aerial Services Cessna 172 flying at ~600 m above ground level. Image centers were geolocated using an onboard GPS synchronized to the camera shutter. Images were collected with ~70–80% overlap along track and 60–70% overlap between tracks. Due to the high flight altitude needed for safe surveying, GPS ground control points could not be used. Instead, four bedrock ridges bounding the glacier were identified in National Elevation Dataset (NED) DEMs and were used to provide supporting ground control.

Aerial images were processed via Agisoft Photoscan Pro into an orthophoto and digital terrain model with a posting of 17 cm px^{-1}. The structure from motion (SfM) DEM has 40.9 points per square meter, with a root mean square error (RMSE) point location uncertainty of 0.7 m. When down-scaled to NED resolution (8.8 m px^{-1}), the SfM model has 13.3 m RMSE vertical offset from NED. Some of this may represent misalignment of images during SfM processing, but this likely reflects physical processes such as rock glacier movement, snow accumulation and thermokarst pond incision. For the purposes of elevation correcting geophysical profiles, the SfM DEM is comparable in absolute elevation with NED, but with much higher spatial resolution.

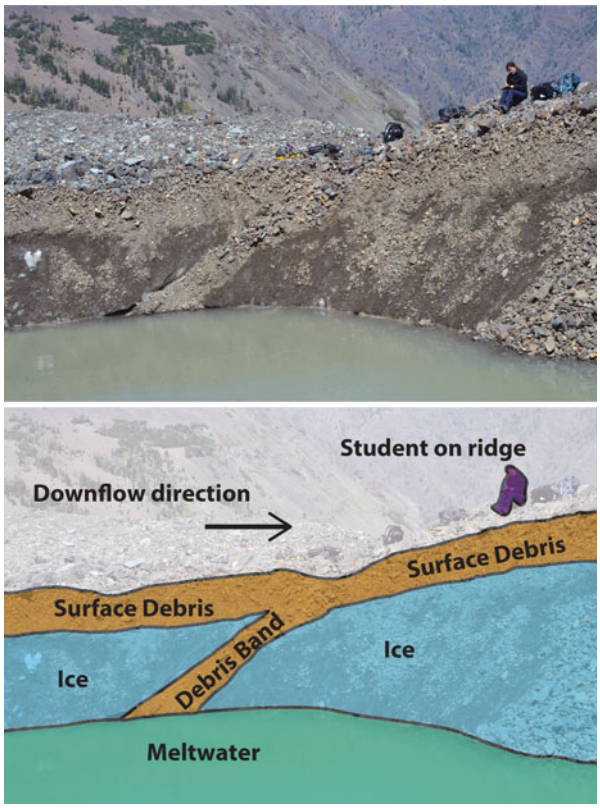

Fig. 2. Image and interpretation of the thermokarst exposure displaying the surface debris layer and an englacial debris band. The ~50 cm thick debris band dips up-glacier, intersecting the surface at an apparent dip of ~30°.

Results

In August 2015, we measured the thermokarst feature to be 40 m wide, exposing the upper 4–5 m of rock glacier stratigraphy in the cirque (Fig. 2). An ice-free surface debris layer 1–1.5 m thick was observed overlying high purity glacial ice. As the ice melted throughout the day, surface debris wasted down the ice surface to cover it. We observed in the thermokarst exposure a debris band extending from the surface debris layer into the subsurface, ~50 cm thick and dipping toward the cirque headwall at an apparent dip of 30°. Upon returning to the thermokarst feature in August 2016 we found it inactive, with most of the meltwater drained and the ice exposures covered completely by debris.

The common midpoint GPR survey (Fig. 3) imaged numerous reflectors at time delays of up to 650 ns. We fit diffraction hyperbolae to 15 of these to solve for the radio wave speed as a function of depth. The shallowest reflector yielded a velocity of 0.116 m ns^{-1} (dielectric constant of $\epsilon' = 6.69$); the remainder of the reflectors produced a range of velocities between 0.15 and 0.17 m ns^{-1}, with a mean value of 0.156 ± 0.014 m ns^{-1} ($\epsilon' = 3.70 \pm 0.33$). We used this value for migrating and depth-converting reflection survey radargrams.

Radar data obtained near the thermokarst pond is shown in Figure 4. In the along-track direction (Figs 4a, b) we resolved at least four reflectors of moderate reflection strength that dip up-glacier at 20–25° and extend semi-continuously up to 30 m depth in the subsurface. In the flow-transverse direction (Figs 4c, d) they are broadly concave-up. The 50 MHz antennas were, for the most part, unable to detect the reflectors. A flat, strong reflector was also imaged at ~40 m depth.

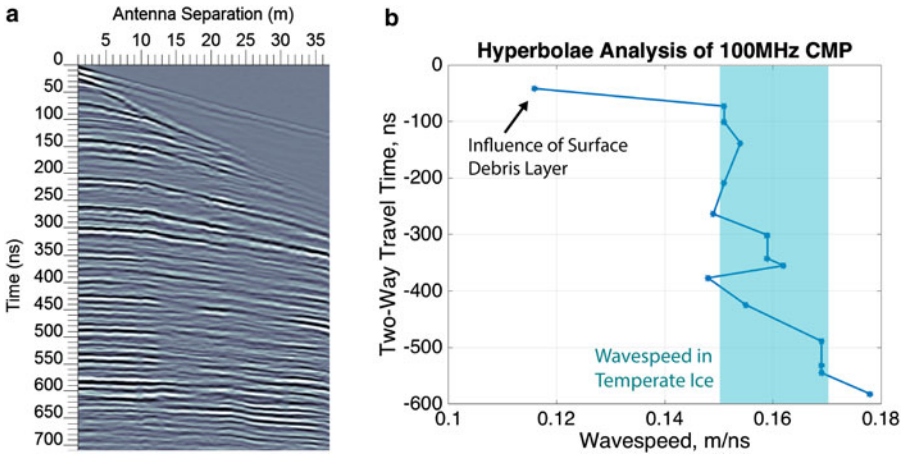

Fig. 3. Common midpoint survey used to determine radio wave speed in the subsurface. (a) Common midpoint radargram. (b) Velocities resulting from common midpoint hyperbolae analysis. Mean velocity = 0.156 m ns^{-1}, a value consistent with temperate glacial ice.

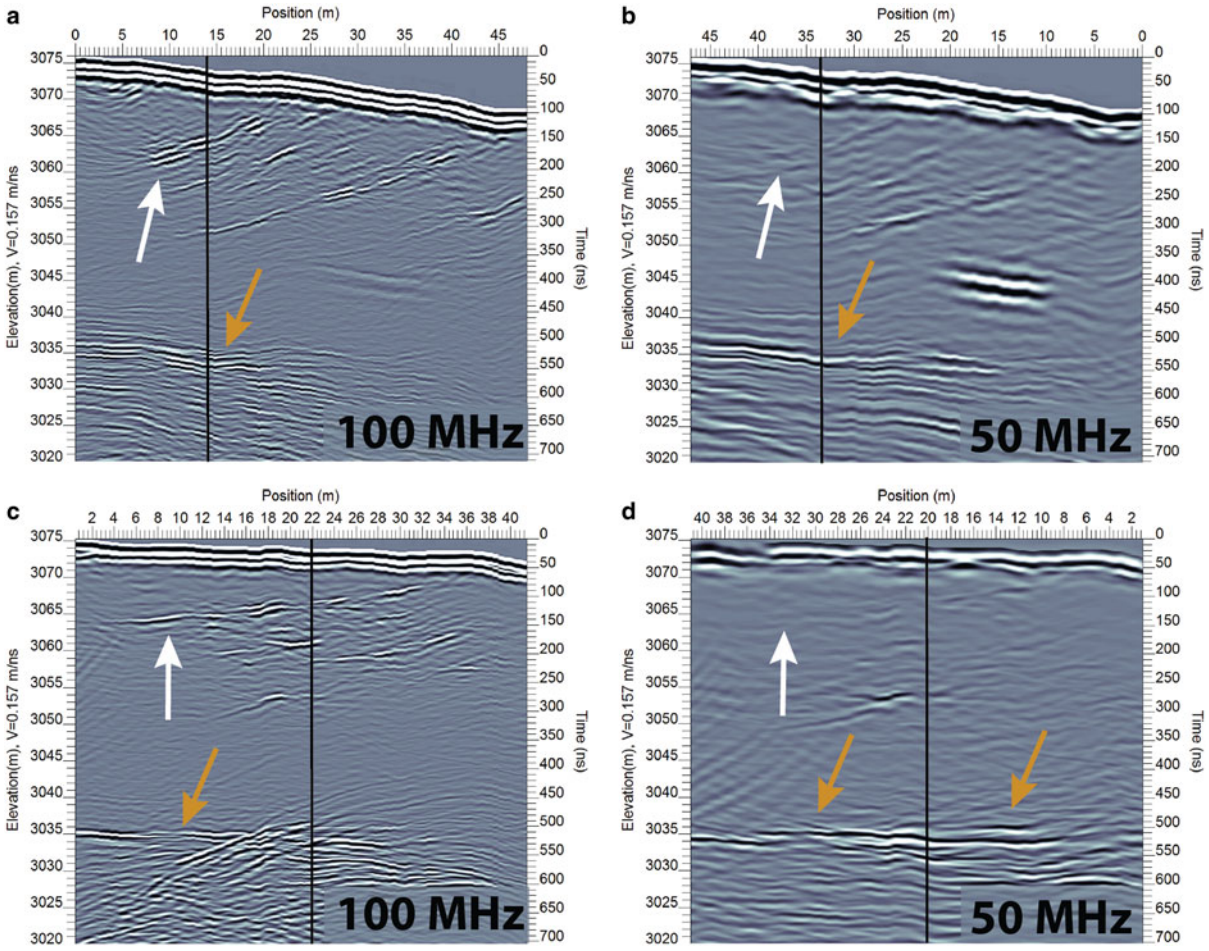

Fig. 4. Radargrams near the thermokarst pond. (a) Profile acquired at 100 MHz in the along-flow direction displaying several dipping reflectors (white arrows). The reflector at 40 m depth may be the base of the rock glacier (brown arrows). Northeast/downglacier is to the right. (b) 50 MHz data also along profile; note that many of the dipping reflectors effectively disappear in the 50 MHz data. (c) Profile acquired at 100 MHz in the flow-transverse direction with several reflectors imaged; one indicated by an arrow has a partial concave-up shape. Northwest is to the right. (d) 50 MHz data also along profile; again, many of the reflectors disappear. The vertical black lines in each panel indicate the point where the longitudinal and transverse profiles intersect. The possible base of the glacier is imaged in both 50 MHz radargrams at ~40 m depth, or 3035 m elevation (orange arrows).

Radar data obtained in the eastern portion of cirque displayed strong, continuous reflectors at depth that resemble a network of nested spoons (Fig. 5). Similar to the reflectors at the other end of the cirque, these intersect the surface at up-glacier dips of 25–35°. However, these are more numerous (11+ reflectors), continuous, intersect the surface near flow-transverse topographic ridges, fully enclose the ice into stratigraphic units, and are strong in both the 50 and 100 MHz data (Fig. 6). The ice units enclosed by the reflectors are typically 2–4 m thick, with the thickest being up to 6–7 m. While the architecture of the reflectors appears similar to nested spoons, there is some complexity including bifurcating reflectors, ice units not in contact with the surface debris layer, and overlapping or disconnected ice units.

The contrast between the complex of reflectors in the east cirque vs the relatively featureless center glacier body can be seen in Figures 5c and 6c. A 110 m long flow-parallel radar profile

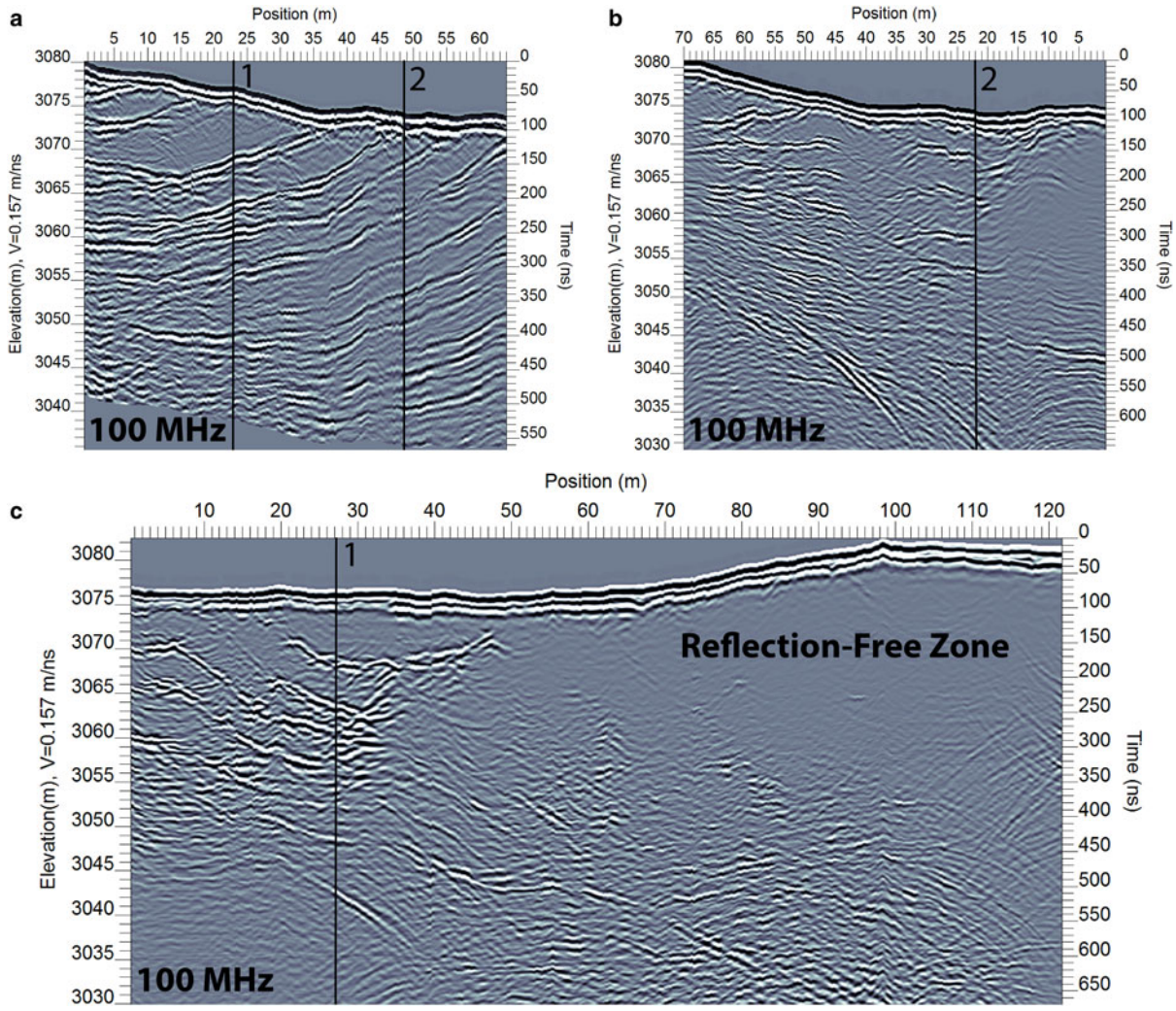

Fig. 5. 100 MHz radargrams acquired on the east side of the cirque. (a) Flow-parallel profile displaying numerous (>6) strong up-glacier dipping reflectors. North by northeast/downglacier is to the right. (b) Flow-transverse profile displaying complex, broken geometry of reflectors. Northwest is to the right. (c) Flow-transverse profile that extends into the center glacier, illustrating how localized the reflector set is; the main glacier body is for the most part reflection-free. In this view we see the reflectors are concave-up, forming a tight nested-spoons geometry. Numbered black lines in each panel indicate the point of intersection between transects. West by northwest is to the right.

acquired down the center of the glacier in the cirque is shown in Figure 7, profile #2016-3. Shallow weak dipping reflectors are observed in 100 MHz but are barely visible in 50 MHz. A strong reflector extends from depths of ~28 m at the up-glacier extreme of the profile to depths of ~55 m where it fades to the noise floor.

We made use of the road crossing the middle section of Galena Creek Rock Glacier to obtain a long radargram across the full width of the glacier (Fig. 8). We observed a zone with very little scattering or reflectors down to a depth of 20–25 m, where there is a strong concave-up reflector. Beneath that there is a zone with increased scattering and another strong concave-up reflector at 35 m depth, beneath which the scattering continues until it fades to noise at about 45 m depth.

Discussion

The velocities found by the common midpoint survey at depth are consistent with high purity glacier ice. Ice in the near-freezing temperature regime has a dielectric constant of 3.1–3.2 (Evans, 1965; Gough, 1972; Johari, 1976). If we assume the andesitic debris has a dielectric constant of $\epsilon' = 8$ similar to basalt or granite (Reynolds, 1997) and use the Maxwell–Garnett mixing formula (Sihvola, 1999) we find based on our measured velocities an ice purity of 80–95%, consistent with Potter (1972)'s observed value of 88–90%. The low velocity/high dielectric constant of $\epsilon' = 6.7$ found for the first reflector is consistent with higher debris content associated with the surface debris layer.

Our interpretation of the GPR survey results are informed by our observations of the thermokarst feature. We interpret the dipping GPR reflectors found at depth in the cirque to be englacial debris bands by analogy to the debris band observed in the thermokarst exposure. The reflectors intersect the surface at up-glacier dip angles similar to that of the debris band, although they become less sloped at depth forming an overall concave-up shape. Their radar properties are also consistent with a similar layer thickness. The fact the reflectors near the pond are imaged well at 100 MHz and poorly at 50 MHz indicates that they are of a thickness range below the resolution of the 50 MHz and within the resolution range of the 100 MHz. At our prescribed velocity of $v = 0.156 \pm 0.014$ m ns^{-1} the theoretical radar resolution $\lambda/4$ (Reynolds, 1997) is 39 ± 2 cm for 100 MHz and 78 ± 3 cm for 50 MHz. The reflectors are thus 37–75 cm in thickness, similar to the 50 cm thickness of the debris band exposed by thermokarst. The reflectors forming a complex at the eastern side of the glacier are, by the same reasoning, likely at least 75 cm thick as they are seen clearly in both 50 and 100 MHz data.

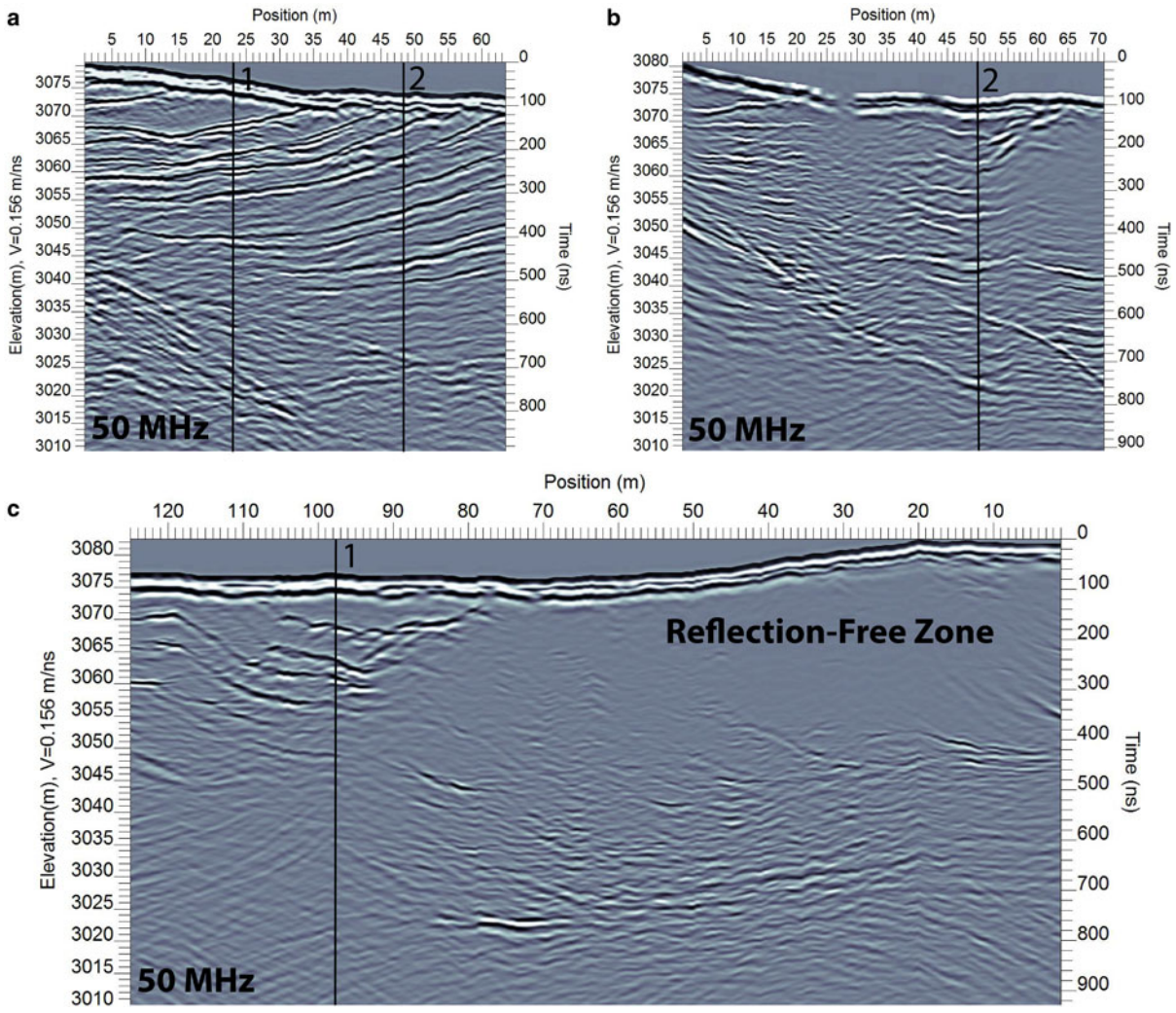

Fig. 6. 50 MHz radargrams acquired on the east side of the cirque, showing that the same reflections are seen at both frequencies. (a) Flow-parallel profile displaying numerous (>6) strong up-glacier dipping reflectors. North by northeast/downglacier is to the right. (b) Flow-transverse profile displaying complex, broken geometry of reflectors. Northwest is to the right. (c) Flow-transverse profile that extends into the center glacier, illustrating how localized the reflector set is; the main glacier body is for the most part reflection-free. In this view we see the reflectors are concave-up, forming a tight nested-spoons geometry. Numbered black lines in each panel indicate the point of intersection between transects. West by northwest is to the right.

Our observations of the relatively clean ice core with intermittent discontinuous debris bands are broadly consistent with Potter (1972)'s model of ice accumulation in the narrow snowfield below the northeast-facing walls of the cirque, with the majority of small-scale debris fall coming to rest on the rock glacier surface at the end of the accumulation zone to form the surface debris layer. We hypothesize that the englacial debris bands were produced by large debris fall events that cover the snowfield and are then subsequently buried by snow/ice accumulation. This is supported by observations by Potter (1972) of a large debris fall that occurred in early spring 1966 and covered 11 000 m^2 of the snowfield and glacier surface with an average 20 cm thickness of debris. This happened to account for two-thirds of the total debris fall observed that year. Areas of the glacier that experience much higher net ice accumulation than debris fall appear relatively clean (center glacier, Fig. 5) or with small, discontinuous debris bands (cirque near thermokarst, Fig. 4), while areas with more significant debris fall develop extensive buried debris bands.

A situation with relatively high debris fall and low ice accumulation may lead to an interesting effect, particularly when large debris falls occur early in the spring season. We present a model for debris and ice accumulation in rock glaciers that we term 'debris-facilitated ice accumulation' (Fig. 9). The cirque snowfield accumulates each winter season from precipitation and wind-packing and has been measured in May 1966 to be up to 6.37 m deep (3.59 m w.e.) (Potter, 1972). However, by the end of summer nearly all of the snowpack is melted and the little that is left is generally located in the southwest corner (northeast-facing slope) of the cirque. Should a large debris fall occur in the early spring, however, it could bury a section of the winter snow pack and insulate it against summer melt. Potter (1972) observed reduced snowpack melt wherever the 1966 debris fall was >7–8 cm in thickness. Over time the buried snow can be incorporated into the rock glacier body as a self-contained ice unit with up to 4 m of ice. The debris thus facilitates net ice accumulation that would not otherwise occur.

There are multiple lines of evidence in support of debris-facilitated ice accumulation as the genesis of the enclosed ice units shown in Figure 5. First, they are in the eastern part of the cirque where the snow field generally melts out completely – i.e. there is little to no 'traditional' net ice accumulation (see Fig. 1b: limited snowfield upslope from ice units). Related is the fact that they are located where a morphological study defined the border between the main rock glacier body and ice-cored moraines (Ackert, 1998, Fig. 1). Second, the ice units are generally of a thickness comparable with that of the available snow water equivalent in

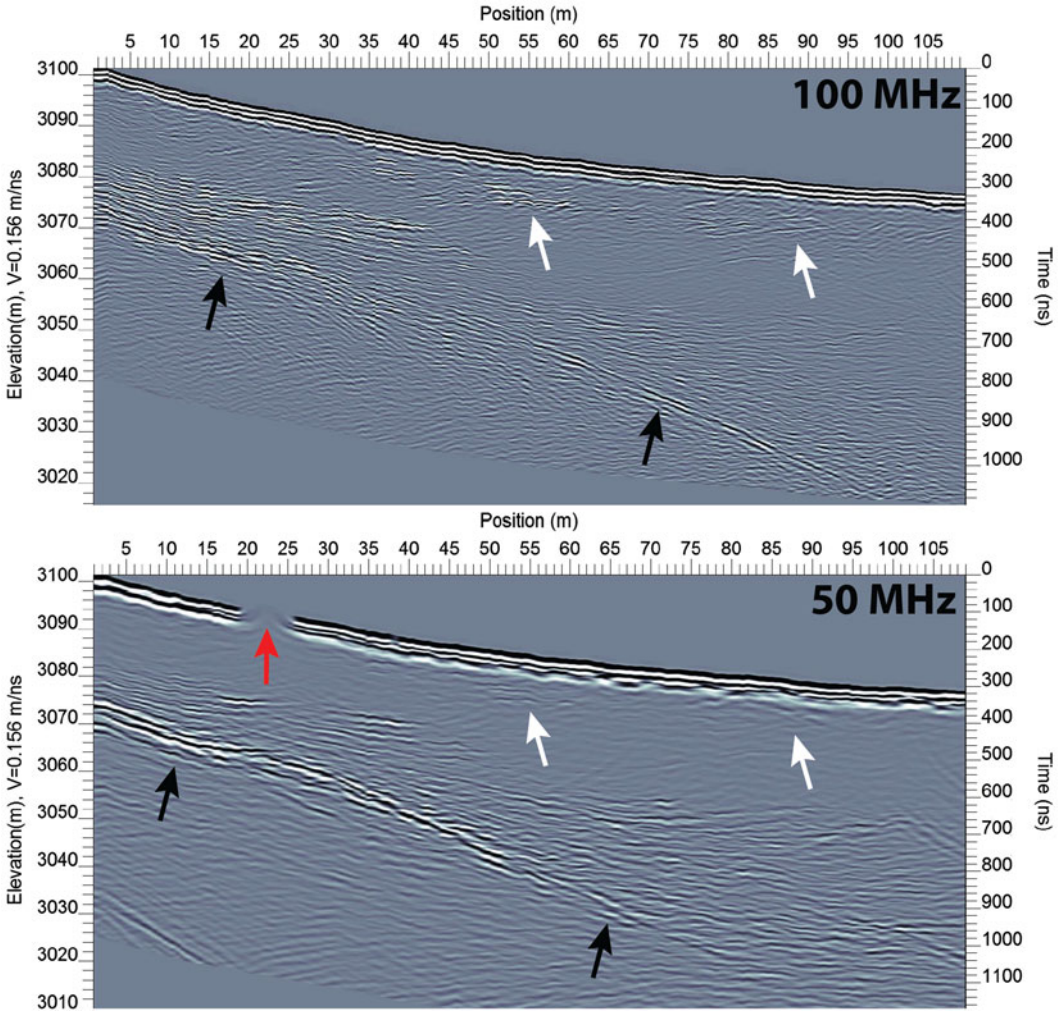

Fig. 7. Flow-parallel profile acquired at 100 and 50 MHz in the center of Galena Creek Rock Glacier, high in the cirque (location mapped in Fig. 1b). White arrows indicate faint dipping reflectors similar to those seen in Figure 4 that are imaged well at 100 MHz and poorly at 50 MHz. Black arrows indicate a reflector at depth interpreted as the base of Galena Creek Rock Glacier. Red arrow indicates missing data in the 50 MHz profile, a result of radar transmitter power loss while acquiring data.

the spring snowpack. Third, the ice units are located directly downslope of large debris cones fed by funneling couloirs (Fig. 1b). Fourth, a large early spring debris fall has been observed in the cirque at Galena Creek Rock Glacier (Potter, 1972) (similar large debris falls have been observed over other rock glaciers, e.g. Haeberli and others, 2006). Finally, the complex structure of randomly overlapping ice units and debris layers can easily be explained by a random process of debris falls.

This proposed debris-facilitated ice accumulation model is very similar to the model presented by Isaksen and others (2000) for periglacially-derived rock glaciers, in which snowdrifts are buried by rock avalanche and then metamorphosed into ice by meltwater entrapment and refreezing. However, we would like to highlight this process as a bridge between the glacially-dominated and periglacially-dominated rock glacier end-members. Note in Figure 5c the transition from the high purity ice core in the center glacier into the interlayered ice bodies and debris layers toward the eastern glacier. As we move toward a more snow/ice-starved system, the thickness and ice-purity of such ice-rich layers would be reduced, leading to a rock glacier end-member similar to that observed by Isaksen and others (2000).

Future studies may test this model by drilling ice cores through the debris and ice layers and providing estimates on their ages based on radiocarbon dating of available organic materials (as in Konrad and others, 1999). Based on the velocities of Potter and others (1998) and the distance between locations where successive layers intersect we estimate they were deposited on a tens of years to century timescale. Because in our model the process of debris-facilitated ice accumulation is stochastic and ongoing we expect the youngest unit to be <100 years old.

The strong reflector observed at depths of ~28 to ~55 m in the center of the cirque (Fig. 7) we interpret as the base of the rock glacier, with the bed dropping away from the headwalls. We also note that a possible basal reflector is imaged at depths of ~40 m depth in the profiles near the thermokarst pond (Fig. 4), which are closer to the western edge of the rock glacier. We conclude that the rock glacier in the cirque is typically 30–50 m thick, and at its thickest is >55 m.

The glacier-wide radargram of the middle section provides a unique view of the large-scale structure of the rock glacier. We interpret the upper 25 m thick zone as the core of pure glacier ice discovered by Potter (1972) and cored by Clark and others (1996). We interpret the deeper scattering zone as a buried layer of debris-rich ice. The second reflector at 35 m depth may be the bedrock contact, but the presence of continued layering and scattering beneath it leads us to interpret it as an internal contact within the rock glacier. Thus, we interpret this as evidence that the rock glacier is at least 35 m thick in this location.

Previous seismic profiling work similarly inferred an ice core 20–25 m thick, but assumed that this was the full thickness of

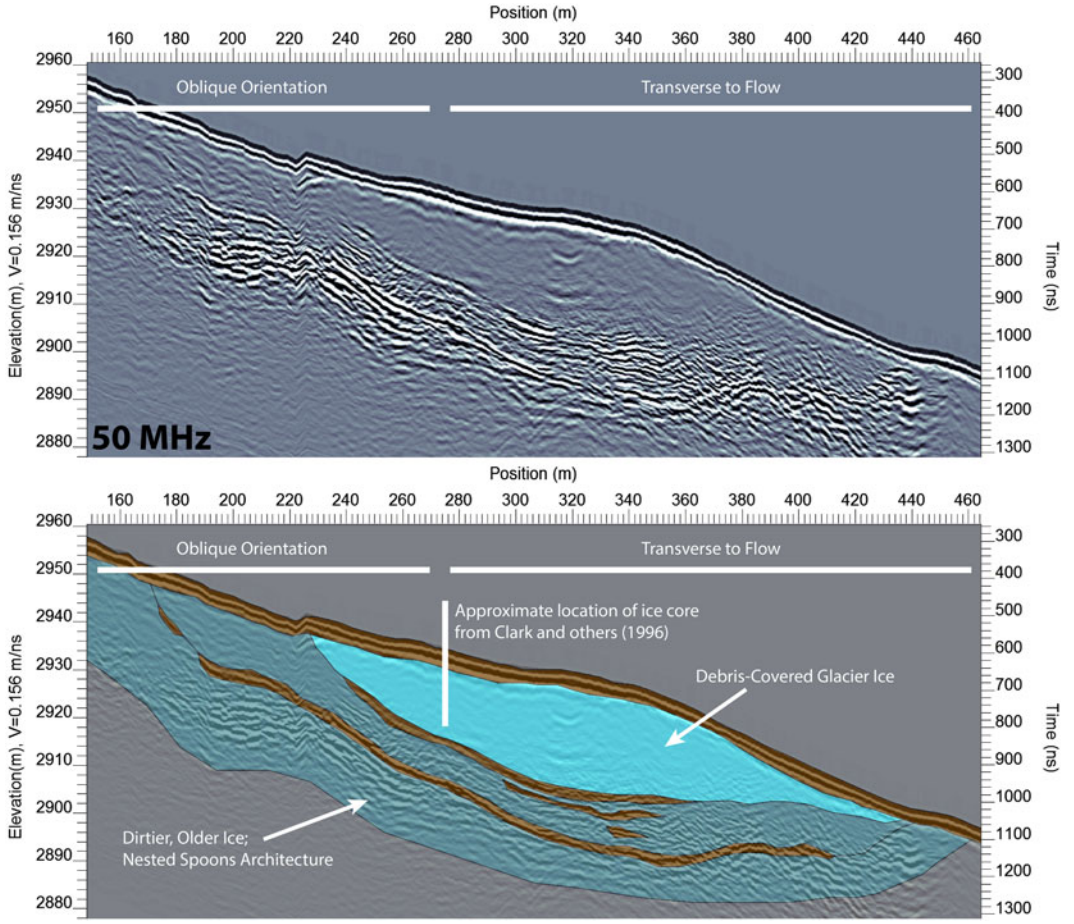

Fig. 8. Mid-glacier radargram (top panel) with overplotted (bottom panel) interpretation. The reflection-free zone down to about 20–25 m depth is interpreted as the clean ice core. The deeper zone which extends past 25–35 m in depth we interpret as a dirty ice-debris mixture. The reflector at 35 m depth may be the bedrock contact. Location is shown in Figure 1a.

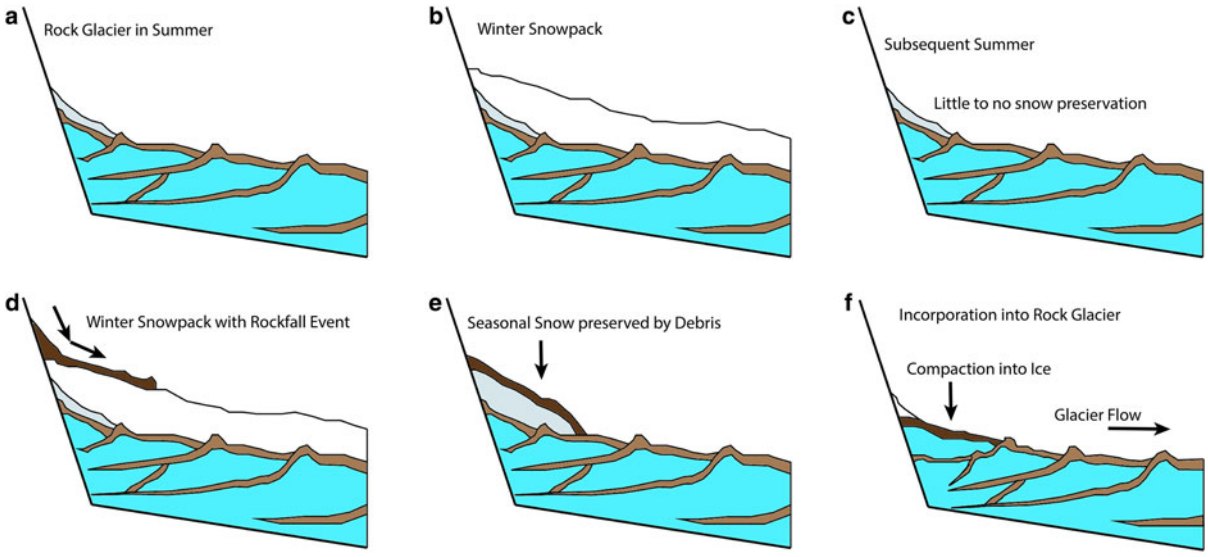

Fig. 9. Cartoon illustrating the model of debris-facilitated ice accumulation. (a–c) In a typical year there is a deep winter snowpack that is mostly ablated by the end of the summer. (d, e) A large debris fall in early spring may bury a part of the snowpack and protect it against summer ablation. (f) Over time the buried snow is incorporated into the rock glacier body as a new ice unit.

the rock glacier; when analysis of measured velocities via Glen's flow law required ice thicknesses on the order of up to 40 m these authors invoked basal sliding (Potter, 1972). We counter that the total thickness of the glacier, including the debris-rich basal layer, is at least 35 m. We also find evidence in the cirque for thicknesses on the order of 30–55 m or greater. Thus we are skeptical that basal sliding need be invoked to explain the motion of this rock glacier.

Our results are somewhat consistent with the model presented by Konrad and others (1999), which predicts a basal debris layer, progressively deposited at the toe of and over-run by the advancing rock glacier. However, we favor the interpretation that the

stratigraphy of the clean ice body overlying the dirty ice layer is indicative of an episodic history of rock glacier accumulation at the area. We favor this interpretation because (1) the basal layer is at least 10 m thick, which is a substantial amount of material to accumulate at the advancing rock glacier front, and (2) Ackert (1998) has previously mapped individual lobes of Galena Creek Rock Glacier indicative of sequential and episodic advances.

The basal dirty ice layer may represent a more ancient and inactive rock glacier episode, the extension of which continues into the lower third of the Galena Creek Valley. It is possible that this layer is more debris-rich due to an accumulation period dominated by debris fall and debris-facilitated accumulation, or merely that most of the ice had ablated from the layer before it was overrun by the younger clean ice body. We interpret the clean ice layer as forming via traditional glacier ice accumulation when the accumulation zone was more active and extensive.

Again, this model may be tested by radiocarbon dating of organic materials found within appropriate rock glacier cores. If our model is correct, the basal material should be significantly older than the overlying ice core, and of similar age to its corresponding rock glacier lobe exposed further down-valley. If the Konrad and others (1999) model is correct, the basal material should be of similar age to the overlying ice core. Numerical modeling of episodic rock glacier production and climate response, i.e. using the model of Anderson and others (2018), may additionally be used to test the validity of this model, and potentially lead to understanding the climate history recorded in rock glacier stratigraphy.

Conclusions

We described through thermokarst exposure observations and GPR data the presence of englacial debris layers produced by large debris falls buried in Galena Creek Rock Glacier. We proposed that these debris falls can additionally facilitate ice accumulation by burying and preserving early spring snowpack which can then be incorporated into the rock glacier as an ice unit. This 'debris-facilitated ice accumulation' effect is likely to be important anywhere there are large and episodic early spring debris falls paired with low or zero net background ice accumulation. It is also a potentially important process bridging the gap between the end-members of purely sedimentary glacial ice and refrozen periglacial ice as the source of rock glacier ice.

We also show that the thickness of the rock glacier in the cirque is 28–55 m and may be greater for some areas; this is a larger value than the 20–25 m thickness estimated by Potter (1972) with seismic methods. We also constrained the internal structure for the middle section of the glacier. We confirmed the presence of a glacial ice core down to a depth of 20–25 m and additionally described a stratigraphy of reflectors we interpret as alternating layers of debris-rich ice and debris near the base of the rock glacier. We speculate that these represent different episodes of rock glacier activity and are thus a potential climate record. The models we present in this work may be verified by future radiocarbon dating of organics in new ice cores recovered from Galena Creek Rock Glacier.

Acknowledgments. This work was funded by the NASA Earth and Space Science Fellowship awarded to Eric Petersen, as well as a UT Austin Jackson School of Geosciences Seed Grant awarded to Cassie Stuurman for the 2016 field season. We thank Robert S. Anderson and an anonymous reviewer for their comments and constructive criticism which have greatly improved the final manuscript. We thank the UT Planetary Geophysics Class of 2015 for their valuable work, including: Ben Cardenas, Stefano Nerozzi, Jim Pharr, William Hoey, Parvathy Prem, Dan Aylward, Jackie Rambo, Logan Schmidt, YeJin Lim and Kian Maharaj. We also thank Starla Talbot for her help in the 2016 field season.

References

Ackert Jr RP (1998) A rock glacier/debris-covered glacier system at Galena Creek, Absaroka Mountains, Wyoming. *Geografiska Annaler Series A*, **80**(3–4), 267–276. doi: 10.1111/j.0435-3676.1998.00042.x.

Anderson RS, Anderson LS, Armstrong WH, Rossi MW and Crump SE (2018) Glaciation of alpine valleys: the glacier – debris-covered glacier – rock glacier continuum. *Geomorphology*, **311**, 127–142. doi: 10.1016/j.geomorph.2018.03.015.

Barsch D (1987) *The Problem of the Ice-cored Rock Glacier*, vol.. 1. Boston: Allen & Unwin.

Berthling I, Etzelmüller B, Isaksen K and Sollid JL (2000) Rock glaciers on Prins Karls Forland. II: GPR soundings and the development of internal structures. *Permafrost and Periglacial Processes*, **11**(4), 357–369. doi: 10.1002/1099-1530(200012)11:4<357::AID-PPP366>3.0.CO;2-6.

Capps SR (1910) Rock glaciers in Alaska. *The Journal of Geology*, **18**(4), 359–375.

Clark DH and 5 others (1996) Old ice in rock glaciers may provide long-term climate records. *Eos*, **77**(23), 217–222. doi: 10.1029/96EO00149.

Clark DH, Steig EJ, Potter Jr N and Gillespie AR (1998) Genetic variability of rock glaciers. *Geografiska Annaler Series A*, **80**(3–4), 175–182. doi: 10.1111/j.0435-3676.1998.00035.x.

Degenhardt JJ and Giardino JR (2003) Subsurface investigation of a rock glacier using ground-penetrating radar: implications for locating stored water on Mars. *Journal of Geophysical Research*, **108**(E4), 1–17. doi: 10.1029/2002JE001888.

Evans S (1965) Dielectric properties of ice and snow–a review. *Journal of Glaciology*, **5**(42), 773–792. doi: 10.3189/S0022143000018840.

Florentine C, Skidmore M, Speece M, Link C and Shaw CA (2014) Geophysical analysis of transverse ridges and internal structure at Lone Peak Rock Glacier, Big Sky, Montana, USA. *Journal of Glaciology*, **60** (221), 453–462. doi: 10.3189/2014JoG13J160.

Gough SR (1972) A low temperature dielectric cell and the permittivity of hexagonal ice to 2 K. *Canadian Journal of Chemistry*, **50**(18), 3046–3051. doi: 10.1139/v72-483.

Haeberli W, Hallet B, Arenson L, Elconin R, Humlum O, Kääb A, Kaufmann V, Ladanyi B, Matsuoka N, Springman S and Mühll D (2006) Permafrost creep and rock glacier dynamics. *Permafrost and Periglacial Processes*, **17**(3), 189–214. doi: 10.1002/ppp.561.

Hauck C, Böttcher M and Maurer H (2011) A new model for estimating subsurface ice content based on combined electrical and seismic data sets. *The Cryosphere*, **5**(2), 453–468. doi: 10.5194/tc-5-453-2011.

Hausmann H, Krainer K, Brückl E and Mostler W (2007) Internal structure and ice content of Reichenkar rock glacier (Stubai Alps, Austria) assessed by geophysical investigations. *Permafrost and Periglacial Processes*, **18**(4), 351–367. doi: 10.1002/ppp.601.

Holt JW, Safaeinili A, Plaut JJ, Head JW, Phillips RJ, Seu R, Kempf SD, Choudhary P, Young DA, Putzig NE, Biccari D and Gim Y (2008) Radar sounding evidence for buried glaciers in the southern mid-latitudes of Mars. *Science*, **322**(5905), 1235–1238. doi: 10.1126/science.1164246.

Isaksen K, Ødegård RS, Eiken T and Sollid JL (2000) Composition, flow and development of two tongue-shaped rock glaciers in the permafrost of Svalbard. *Permafrost and Periglacial Processes*, **11**(3), 241–257. doi: 10.1002/1099-1530(200007/09)11:3<241::AID-PPP358>3.0.CO;2-A.

Johari GP (1976) The dielectric properties of H_2O and D_2O ice Ih at MHz frequencies. *The Journal of Chemical Physics*, **64**(10), 3998–4005. doi: 10.1063/1.432033.

Konrad SK and 6 others (1999) Rock glacier dynamics and paleoclimatic implications. *Geology*, **27**(12), 1131. doi: 10.1130/0091-7613(1999)027<1131:RGDAPI>2.3.CO;2.

Mackay SL, Marchant DR, Lamp JL and Head JW (2014) Cold-based debris-covered glaciers: evaluating their potential as climate archives through studies of ground-penetrating radar and surface morphology. *Journal of Geophysical Research: Earth Surface*, **119**(11), 2505–2540. doi: 10.1002/2014JF003178.

Mahaney WC, Miyamoto H, Dohm JM, Baker VR, Cabrol NA, Grin EA and Berman DC (2007) Rock glaciers on Mars: Earth-based clues to Mars

recent paleoclimatic history. *Planetary and Space Science*, **55**(1–2), 181–192. doi: 10.1016/j.pss.2006.04.016.

Maurer H and Hauck C (2007) Geophysical imaging of alpine rock glaciers. *Journal of Glaciology*, **53**(180), 110–120.

Nye JF (1957) The distribution of stress and velocity in glaciers and ice-sheets. *Proceedings of the Royal Society A*, **239**(1216), 113–133

Outcalt SI and Benedict JB (1965) Photo-interpretation of two types of rock glacier in the Colorado front range, USA. *Journal of Glaciology*, **5**(42), 849–856. doi: 10.3189/S0022143000018918.

Petersen EI, Holt JW and Levy JS (2018) High ice purity of martian lobate debris aprons at the regional scale: Evidence from an orbital radar sounding survey in Deuteronilus and Protonilus Mensae. *Geophysical Research Letters*, **45**(21), 11595–11604. doi: 10.1029/2018GL079759.

Potter N (1972) Ice-cored rock glacier, Galena Creek, northern Absaroka Mountains, Wyoming. *Geological Society of America Bulletin*, **83**(10), 3025–3058. doi: 10.1130/0016-7606(1972)83[3025:IRGGCN]2.0.CO;2.

Potter Jr N and 6 others (1998) Galena Creek rock glacier revisited – new observations on an old controversy. *Geografiska Annaler Series A*, **80**(3–4), 251–265.

Rangecroft S, Harrison S and Anderson K (2015) Rock glaciers as water stores in the Bolivian Andes: an assessment of their hydrological importance. *Arctic, Antarctic, and Alpine Research*, **47**(1), 89–98. doi: 10.1657/AAAR0014-029.

Reynolds JM (1997) *An Introduction to Applied and Environmental Geophysics*. Chichester, New York: Wiley.

Sihvola AH (1999) *Electromagnetic Mixing Formulas and Applications*. IET, London, UK.

Smedes H and Prostka H (1972) Stratigraphic framework of the Absaroka Volcanic Supergroup in the Yellowstone National Park region. USGS Numbered Series 729-C.

Squyres SW (1978) Martian fretted terrain: flow of erosional debris. *Icarus*, **34**(3), 600–613. doi: 10.1016/0019-1035(78)90048-9.

Steig EJ, Clark DH, Potter Jr N and Gillespie AR (1998) The geomorphic and climatic significance of rock glaciers. *Geografiska Annaler Series A*, **80**(3–4), 173–174. doi: 10.1111/j.0435-3676.1998.00034.x.

Wahrhaftig C and Cox A (1959) Rock glaciers in the Alaska Range. *Geological Society of America Bulletin*, **70**(4), 383. doi: 10.1130/0016-7606(1959)70[383:RGITAR]2.0.CO;2.